Electronic Supplementary Material (ESI) for Inorganic Chemistry Frontiers.

Supporting Information

Stabilizing V_2O_3 in carbon nanofiber flexible films for ultrastable potassium storage

*Ge Yao,[a,b,c,] Minxi Lin,[a,b,c,] Jie Yang,[a,b,c,] Lingzhi Wei,[a,b,c,] Heling Niu,[c] Qiquan Luo,[*a] Fangcai Zheng [*a,b,c] and Qianwang Chen[d]*

[a] Institutes of Physical Science and Information Technology, Key Laboratory of Structure and Functional Regulation of Hybrid Materials, Anhui University, Hefei, Anhui 230601, People's Republic of China.
[b] Anhui Graphene Engineering Laboratory, Anhui University, Hefei, 230601, China. Key Laboratory of Functional Inorganic Material Chemistry of Anhui Province,
[c] Energy Materials and Devices Key Laboratory of Anhui Province for Photoelectric Conversion, Anhui University, Hefei, 230601, China
[d] Hefei National Laboratory for Physical Science at Microscale, Department of Materials Science & Engineering, University of Science and Technology of China, Hefei, Anhui, 230026, People's Republic of China.
[†] E-mail: zfcai@mail.ustc.edu.cn; qluo@ustc.edu.cn.

Content

Experiment

Material Synthesis: All chemicals used in the experiment are analytical grade and were from Macklin without any further purification. The flexible films, V_2O_3/CNF, were prepared by electrospinning method within thermal calcination. The vanadyl acetylacetonate ($V(acac)_3$, 0.2786 g) was first dissolved in DMF to obtain a clear solution. Next, polyacrylonitrile (PAN, FW=150000) was added and continuously stirred overnight at room temperature to form the homogenous solution. Then, an electrospinning process was carried out with the voltage of 30 KV and a distance of 18 cm. Finally, the obtained film was calcined in N_2 atmosphere at 800 °C for 2 h with 10 °C/min. The final product was recorded as vanadium-oxide/carbon nanofibers (V_2O_3/CNF). The contrastive sample, carbon nanofibers (C), was prepared by the same method with only PAN. And the vanadium-oxide (V_2O_3) was prepared through the $V(acac)_3$ powder with the same calcination conditions.

Material Characterization: XRD measurements were performed using X-ray powder diffraction (XRD, Rigaku Co, Japan, D/MAX-γA) with Cu Kα radiation (λ=1.54056 Å) at a scan rate of 8 ^{o} min^{-1}. The morphologies were systematically characterized by scanning electron microscopy (SEM, JEOL JSM-6700 M) and transmission electron microscopy (TEM, Hitachi H-800) coupled with energy dispersive X-ray (EDX) analysis. TGA was performed on TGA-5500 in the air from room temperature to 850 °C with a temperature ramp of 10 °C min^{-1}. The XPS was performed using (XPS, ESCALAB 250). Raman spectra were tested using Confocal Laser MicroRaman Spectrometer (Via-Reflex/inVia-Reflex).

Electrochemical Measurements: The electrochemical properties were evaluated with coin-type cells assembled in an argon-filled glove box (O_2 and H_2O < 0.1 ppm). The V_2O_3/CNF flexible films were directly used as working electrode with a loading about 1.15 mg cm^{-2} and the 0.636 cm^2 of average area. The half cells with 2032 coin-type were assembled using potassium as counter electrode and glass fiber as separator. The electrolyte was 3 M KFSI dissolved in a mixed solution of ethylene carbonate/propylene carbonate (EC/DEC, 1:1 by volume). Galvanostatic charge/discharge tests were carried out on the Neware CT3008W in the voltage range of 0.01−3.0 V. And the electrochemical performance of V_2O_3@CNF electrode was based the total mass of V_2O_3@CNF. Electrochemical impedance spectroscopy (EIS) and Cyclic voltammetry (CV) test were conducted on CHI760E electrochemical workstation. The CV tests were carried out in the potential range of 0.01−3.0 V at different scanning rate.

DFT calculation: All calculations were performed using the plane-wave periodic density functional method (DFT) in the Vienna *ab initio* simulation package (VASP) [1,2]. The electron ion interaction was described with the projector augmented wave (PAW) method [3,4]. The electron exchange and correlation energy were treated within the generalized gradient approximation (GGA) in the form of the Perdew-Burke-Ernzerhof (PBE) functional [5]. The cut-off energy was set up to 500 eV. The force convergence was set to be lower than 0.02 eV/Å, and the total energy convergence was set to be smaller than 10^{-5} eV. Electron smearing of σ = 0.05 eV was used following the the Gaussian scheme.

The Brillouin zone was sampled using Monkhorst–Pack scheme with a k-point mesh of 3 × 3 × 1 centered at the Γ-centered point for the structural relaxation, and 3 × 3 × 1 k-point mesh was used for the static calculations of charge density difference and Bader charge, 9 × 9 × 1 k-point mesh was used for the static calculations of density of states [6]. The structure relaxation was continued until the forces on all the atoms are converged to less than 0.02 eV/Å.

The crystal data of the initial structure comes from the Crystallographic database following article [7]. The optimized lattice constants of graphene and V_2O_3 are 2.52 and a=c=5.12 Å, c= 13.87 Å, where the value of c/a was 2.70. The U parameter was set at 2.68 for V d-electrons [8]. Spin polarized calculations (collinear) were performed (ISPIN=2). Taking into account the paramagnetic characteristics of vanadium oxide where the magnetic moment of vanadium atoms was set to 2μB and the others to 0μB [9,10]. Zero damping DFT-D3 method of Grimme.

The slab model of the most stable V_2O_3 (0001) surface contains nine atomic layers in thickness with 3 bottom layers fixed while relaxing other atoms besides, and a 2 × 2 supercell in the lateral plane is adopted. Graphene with a 4 × 4 supercell. The lattice mismatch is about 1.35%. The vacuum slab was set up to 12 Å.

Considering previous studies on vanadium oxide and the actual preparation conditions and terminations, a (0001) surface with a pure-oxygen exposure terminations and a few V=O terminations were used [11-14].

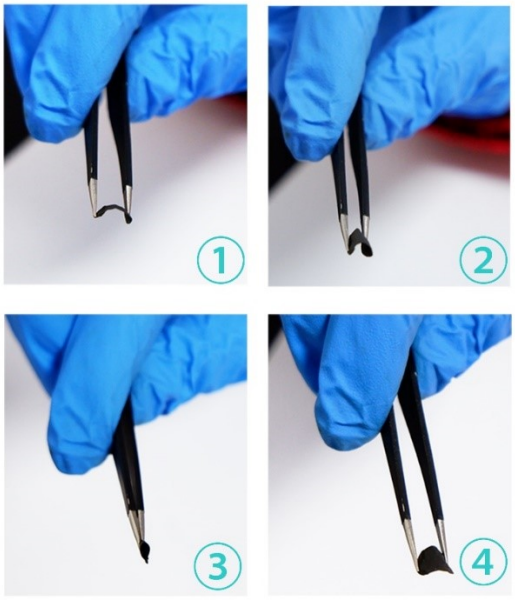

Figure S1. Flexibility of the V_2O_3/CNF film.

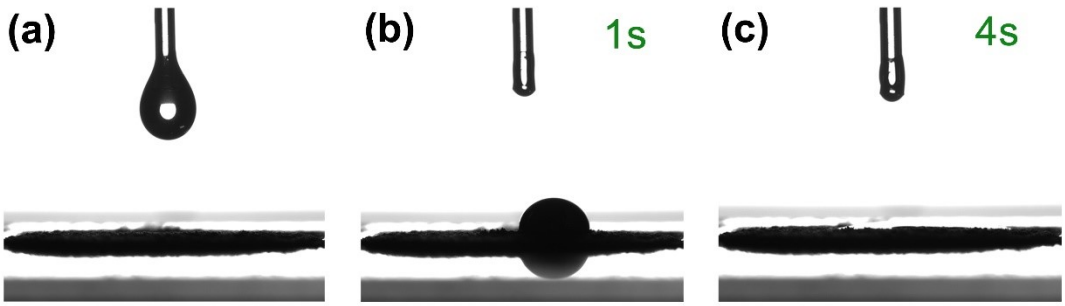

Figure S2. (a), (b), (c) Wettability of the C with electrolyte. C electrode materials cannot be quickly and completely infiltrated by electrolyte.

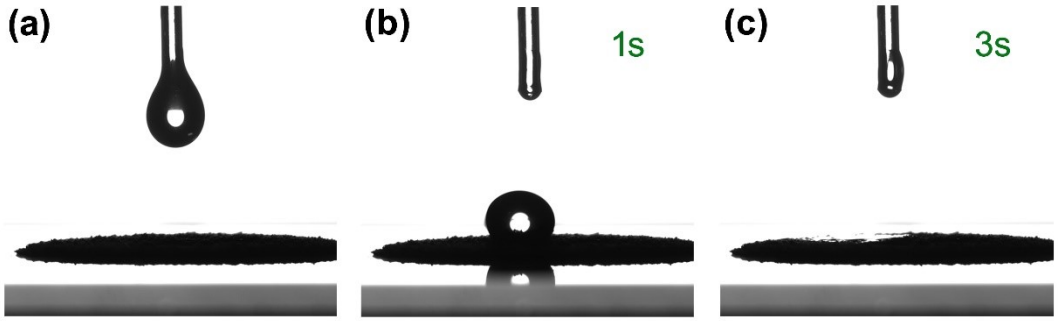

Figure S3 (a), (b), (c) Wettability of the V_2O_3 with electrolyte. V_2O_3 electrode materials cannot be quickly and completely infiltrated by electrolyte.

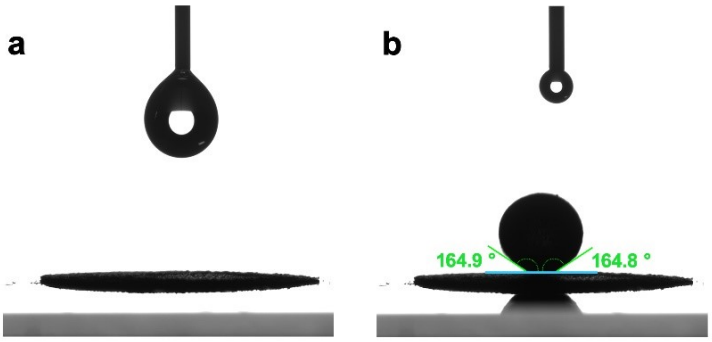

Figure S4. (a), (b) Wettability of the C with H_2O.

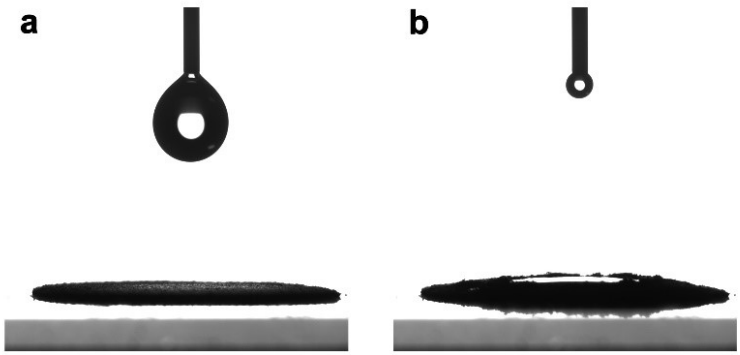

Figure S5. (a), (b) Wettability of the V_2O_3 with H_2O.

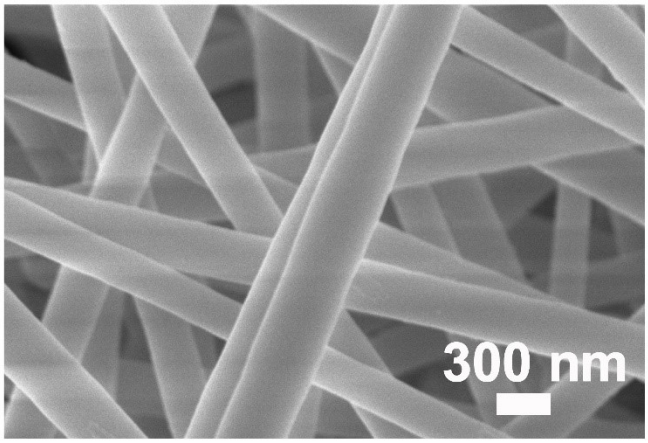

Figure S6. SEM image for the precursor film of V_2O_3/CNF.

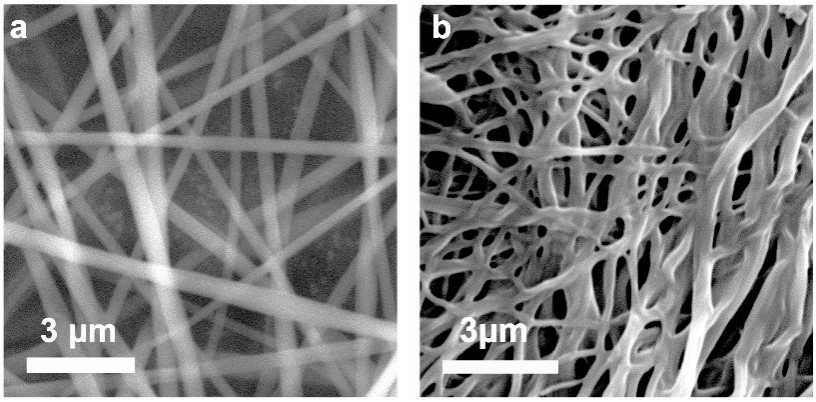

Figure S7. SEM image for the a) precursor film of C and b) C.

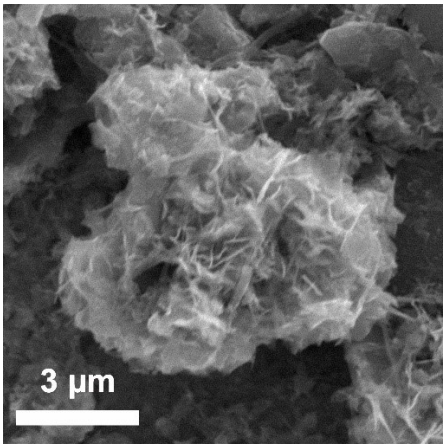

Figure S8. SEM image for theV_2O_3.

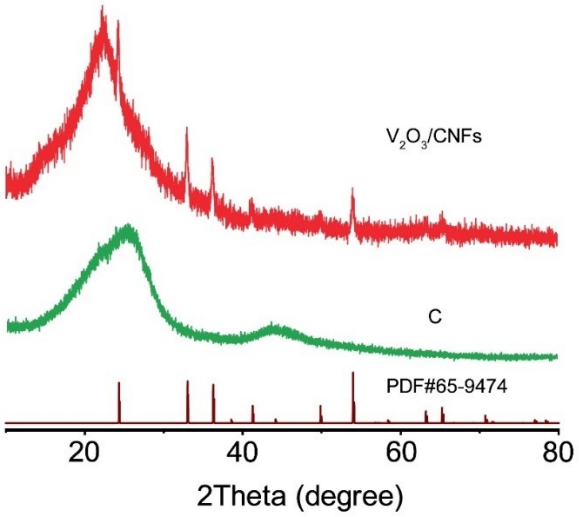

Figure S9. XRD pattern of V_2O_3/CNF and C.

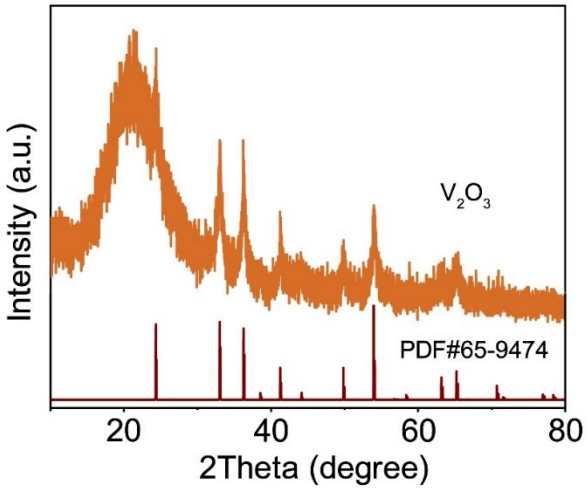

Figure S10. XRD pattern of V_2O_3.

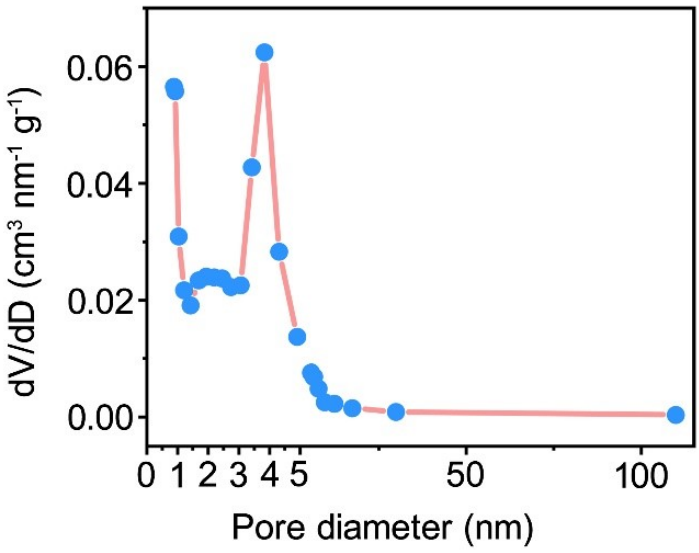

Figure S11. Pore distributions curves of V_2O_3/CNF.

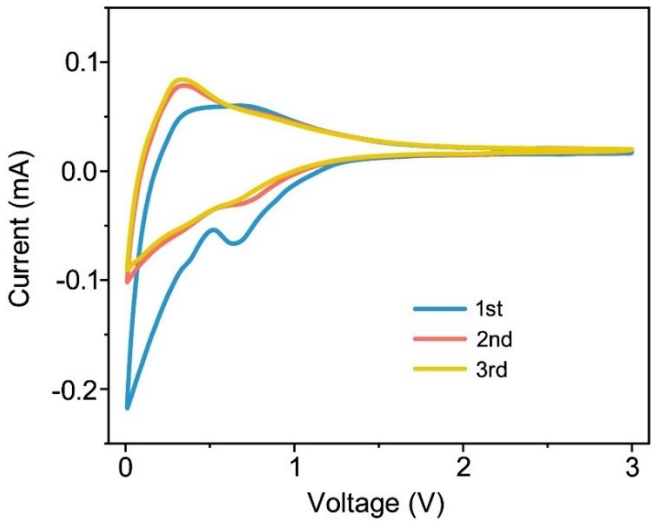

Figure S12. CV curves of C electrode.

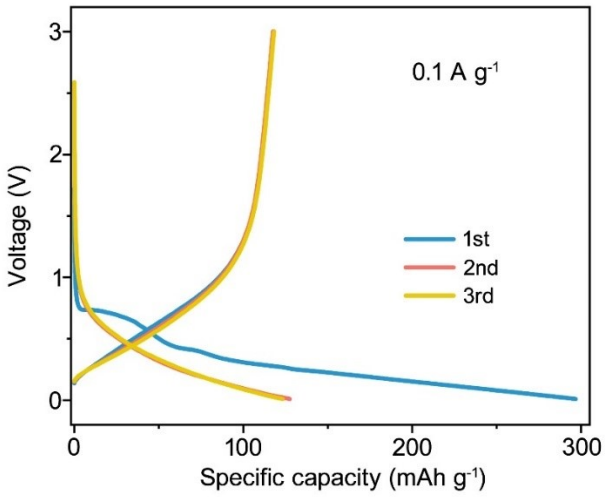

Figure S13. Charge-discharge profiles of C electrode at 0.1 A g^{-1} for initial three cycles.

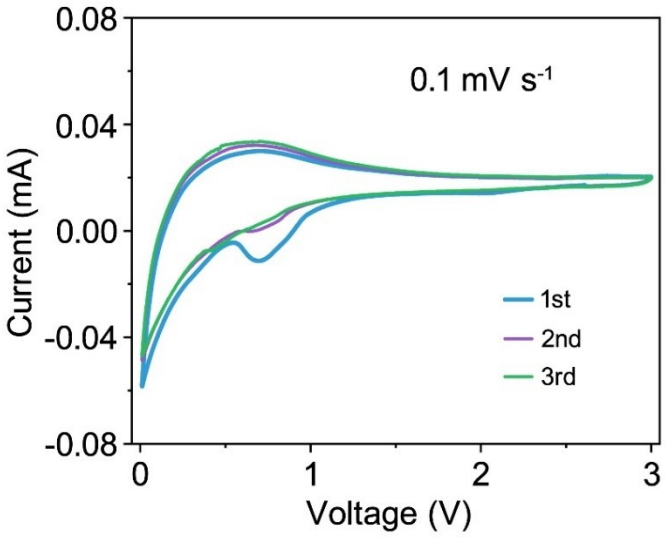

Figure S14. CV curves of V_2O_3 electrode.

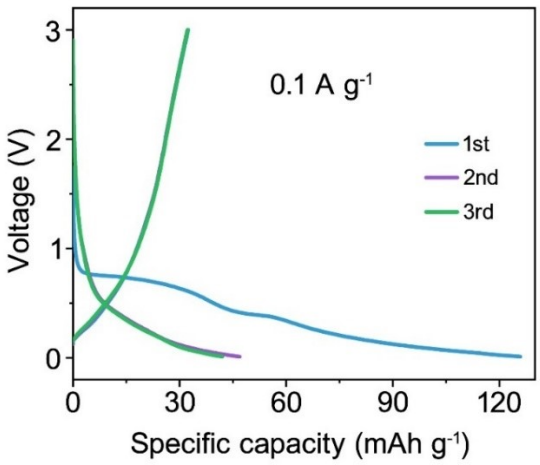

Figure S15. Charge-discharge profiles of V_2O_3 electrode at 0.1 A g^{-1} for initial three cycles.

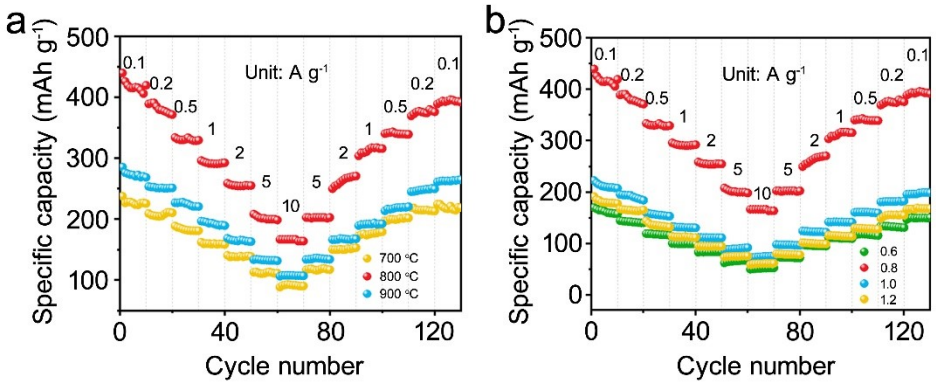

Figure S16. (a) Rate performance of V_2O_3/CNF at different calcination temperature; (b) Rate performance of V_2O_3/CNF with different content of raw material vanadium.

From Figure S16a, the samples at 800 °C had the best performance, so 800 °C was the best temperature for the formation of the samples. And from Figure S16b, the materials prepared with 0.8 mmol had the best electrochemical properties. Thus, the 800 °C with the initial raw material of 0.8 mmol are the the best synthesis condition for the V_2O_3/CNF.

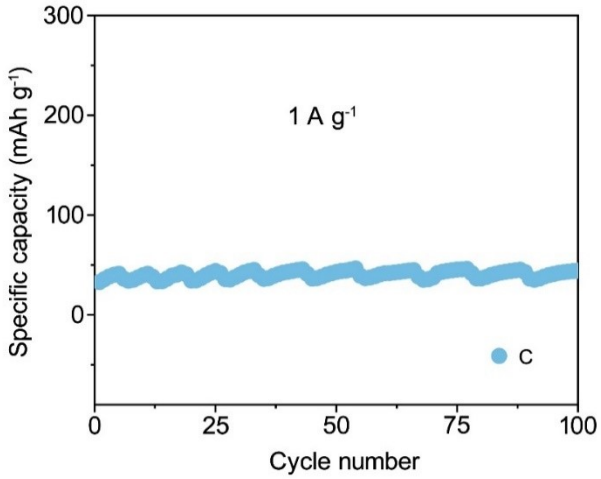

Figure S17. Cycle life of C electrode at 1 A g^{-1}.

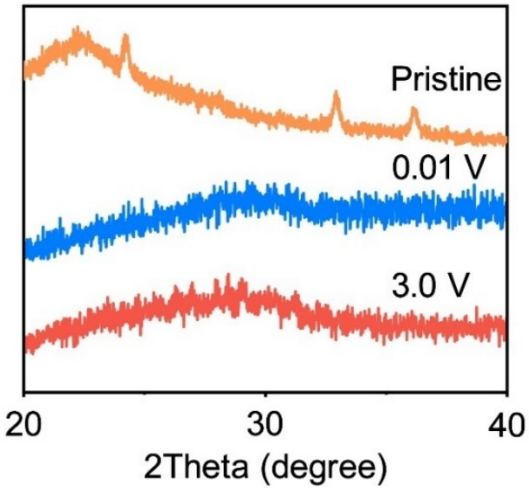

Figure S18. Ex-situ XRD patterns of V_2O_3/CNF at the first cycle.

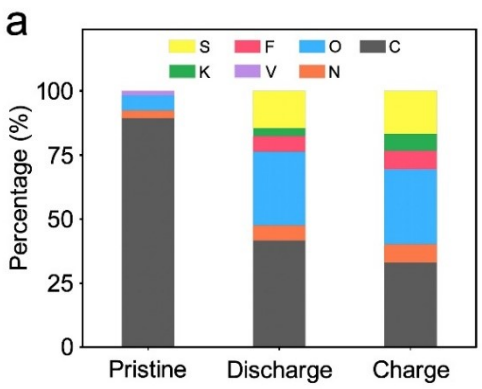

b

	Pristin(%)	Dischar.(%)	Char.(%)
S		14.61	16.79
K		2.97	6.56
F		6.1	7.17
C	89.32	41.63	33.04
O	5.89	28.73	29.08
N	3	5.89	7.14
V	1.79	0.07	0.24

Figure S19. (a), (b) Element content information of V_2O_3/CNF at different state.

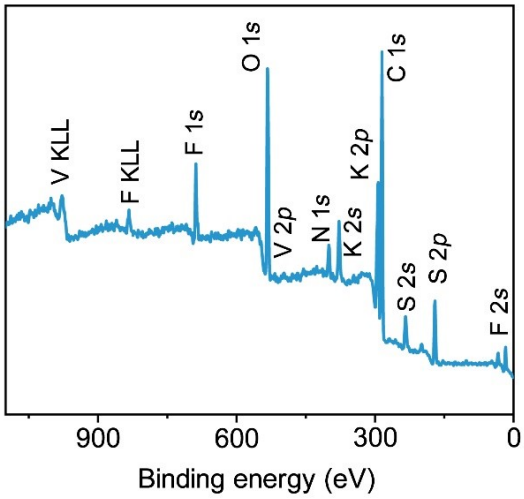

Figure S20. XPS of discharged V_2O_3/CNF.

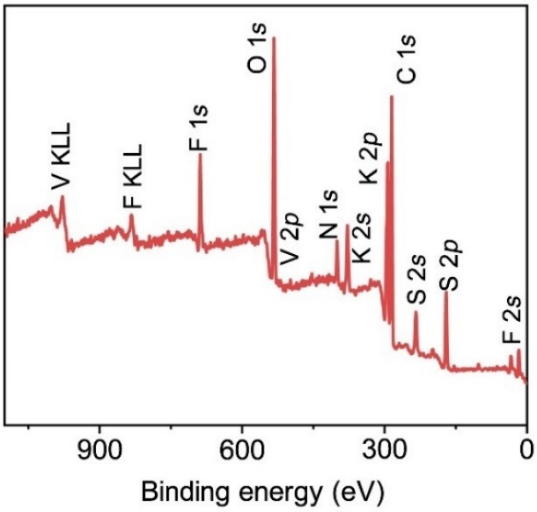

Figure S21. XPS of charged V_2O_3/CNF.

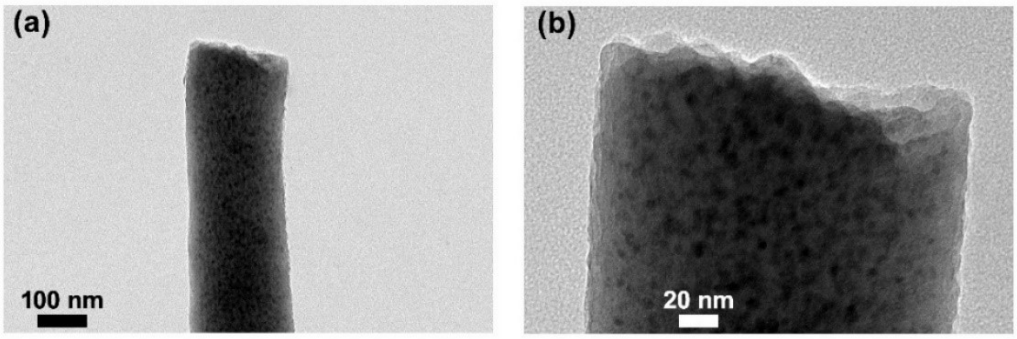

Figure S22. Partially enlarged TEM images of V_2O_3/CNF film after rate cycles.

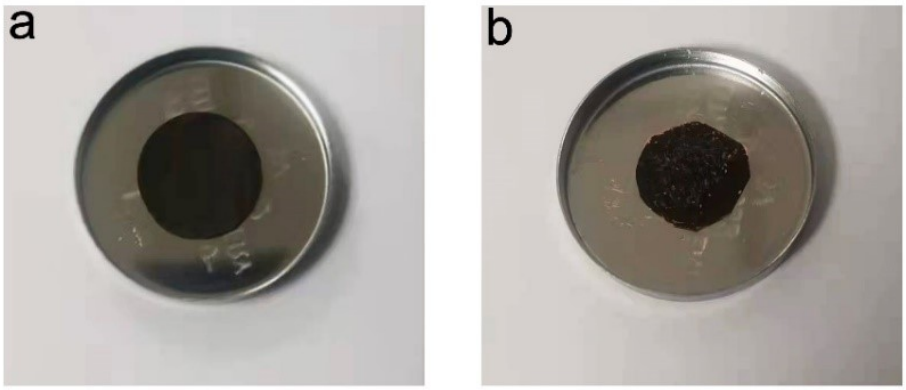

Figure S23. (a) Photo of V_2O_3@CNF electrode at pristine, (b) Photo of V_2O_3@CNF electrodes after cycling.

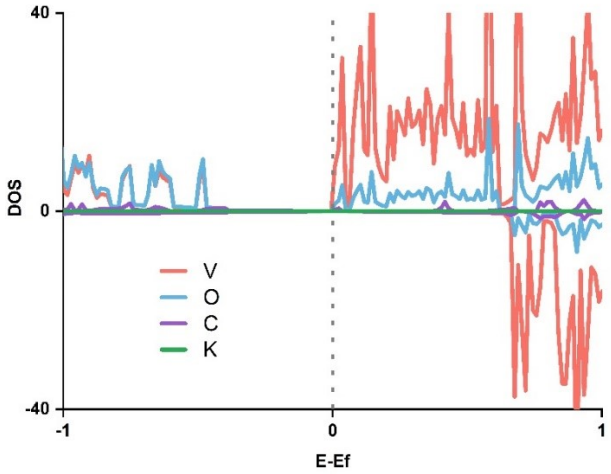

Figure S24. Local Density-of-States of each element for the V_2O_3/C without C-O-V bond.

Table S1. Electrochemical performance of different anode materials on potassium ion battery

Materials	**Rate capacity (mAh g^{-1})**	**Cycle life**	**reference**
carbons	133 at 5 A g^{-1}	the retention of 81% at 1 A g^{-1} over 400 cycles	**15**
flower like-NiS_2	190 at 2 A g^{-1}	239 mAh g^{-1} after 500 cycles at 1 A g^{-1}	**16**
CuP_2/Cu nanowire	101 at 10 A g^{-1},	392 mAh g^{-1} with retention of 99.5% after 50 cycles at 0.1 A g^{-1}	**17**
$MnCo_2O_4$	152 at 1A g^{-1}	126 mAh g^{-1} over 200 cycles at 0.1A g^{-1}	**18**
Co_3O_4@N−C	80 at 2 C	213 mAh g^{-1} after 740 cycles at 0.5 A g^{-1},	**19**

Bi@N-CNCs	235.5 at 10 A g^{-1},	327.5 mAh g^{-1} after 300 cycles at 1 A g^{-1}; 224 mAh g^{-1} with retention of 95.3% at 5 A g^{-1} over 1200 cycles	**20**
Co_3Se_4 QD	154 at 5 A g^{-1},	407 mAh g^{-1} after 550 cycles at 0.1 A g^{-1}; 200 mAh g^{-1} at 1 A g^{-1} after 10000 cycles	**21**
Bi_2MoO_6	165.3 at 0.5 A g^{-1}	121.7 mAh g^{-1} after 600 cycles at 0.1 A g^{-1}	**22**
CuS_2@NC	257 at 6 A g^{-1}	317 mAh g^{-1} after 1200 cycles at 1 A g^{-1}	**23**
soft carbon	115 at 5.0 A g^{-1}	the retention of 92.4% at 1.0 A g^{-1} after 1000 cycles	**24**
Cu_3P	-	174 mA h g^{-1} at 1 A g^{-1} after 300 cycles	**25**
BiSb@TCS	119.3 at 6 A g^{-1}	181 mAh g^{-1} after 5700 cycles at 2 A g^{-1},	**26**

V_2O_3@C	116.6 at 5 A g^{-1}	147.9 mAh g^{-1} after 1800 cycles at 2 A g^{-1}	**27**
VO/C	104 at 15 A g^{-1}	345 mAh g^{-1} at 0.1 A g^{-1} after 400 cycles; 241 mAh g^{-1} at 1 A g^{-1}over 1000 cycles	**28**
V_2O_3/CNF	175 at 10 A g^{-1}	380 mAh g^{-1} after 500 cycles at 0.1 A g^{-1}; the retention of 98% after 2500 cycles at 1 A g^{-1}	**This work**

Table S2. Coulombic efficiency of the V_2O_3/CNF in initial five cycles.

Cycle number	Coulombic efficiency (%)
1	27.9
2	86.7
3	95.6
4	98.4
5	99.2

Table S3. Bader charge analysis of V_2O_3/CNF film with C-O-V bond

No. /Element	V	O	C	K
Sun	53.50	255.11	123.26	8.13
Gains and Losses	-14.50	40.89	-0.74	-0.87

Reference

1 G. Kresse and J. Furthmiiller, Efficiency of ab-initio total energy calculations for metals and semiconductors using a plane-wave basis set, *Comp. Mater. Sci.* , 1996, **6**, 15-50.

2 G. Kresse and J. Furthmu¨ller, Efficient iterative schemes for ab initio total-energy calculations using a plane-wave basis set, *Phys. Rev. B*, 1996, **54**, 11169-11186.

3 P. E. Blochl, Projector augmented-wave method, *Phys Rev B Condens Matter*, 1994, **50**, 17953-17979.

4 G. Kresse and D. Joubert, From ultrasoft pseudopotentials to the projector augmented-wave method, *Phys. Rev. B*, 1999, **59**, 1758-1775.

5 John P. Perdew, Kieron Burke and M. Ernzerhof, Generalized Gradient Approximation Made Simple, *Phys. Rev. Lett.*, 1996, **77**.

6 S. Grimme, J. Antony, S. Ehrlich and H. Krieg, A consistent and accurate ab initio parametrization of density functional dispersion correction (DFT-D) for the 94 elements H-Pu, *J Chem Phys*, 2010, **132**, 154104.

7 Patrick Rozier, Alicja Ratuszna and J. Galy., Comparative Structural and Electrical Studies of V_2O_3 and $V_{2-x}Ni_xO_3$ ($0<x< 0.75$) Solid Solution, *Z. Anorg. Allg. Chem.*, 2002, **628**, 1236-1242.

8 R. Tran, X.-G. Li, S. P. Ong, Y. Kalcheim and I. K. Schuller, Metal-insulator transition in V_2O_3 with intrinsic defects, *Phys. Rev. B*, 2021, **103**, 075134.

9 L. Hu, C. Xie, S. J. Zhu, M. Zhu, R. H. Wei, X. W. Tang, W. J. Lu, W. H. Song, J. M. Dai, R. R. Zhang, C. J. Zhang, X. B. Zhu and Y. P. Sun, Unveiling the

mechanisms of metal-insulator transitions in V_2O_3: The role of trigonal distortion, *Phys. Rev. B*, 2021, **103**, 085119.

10 A. S. M. Jonayat, A. Kramer, L. Bignardi, P. Lacovig, S. Lizzit, A. C. T. van Duin, M. Batzill and M. J. Janik, A first-principles study of stability of surface confined mixed metal oxides with corundum structure (Fe_2O_3, Cr_2O_3, V_2O_3), *Phys Chem Chem Phys*, 2018, **20**, 7073-7081.

11 F. E. Feiten, J. Seifert, J. Paier, H. Kuhlenbeck, H. Winter, J. Sauer and H. J. Freund, Surface structure of V_2O_3(0001) revisited, *Phys Rev Lett*, 2015, **114**, 216101.

12 F. E. Feiten, H. Kuhlenbeck and H.-J. Freund, Surface Structure of V_2O_3(0001): A Combined I/V-LEED and STM Study, *J. Phys. Chem. C*, 2015, **119**, 22961-22969.

13 F. Pfuner, J. Schoiswohl, M. Sock, S. Surnev, M. G. Ramsey and F. P. Netzer, The metal–insulator transition in V_2O_3(0001) thin films: surface termination effects, *J. Phys.-Condens. Mat.*, 2005, **17**, 4035-4047.

14 G. Kresse, S. Surnev, J. Schoiswohl and F. P. Netzer, V_2O_3(0001) surface terminations: a density functional study, *Surface Science*, 2004, **555**, 118-134.

15 X. Ma, N. Xiao, J. Xiao, X. Song, H. Guo, Y. Wang, S. Zhao, Y. Zhong and J. Qiu, Nitrogen and phosphorus dual-doped porous carbons for high-rate potassium ion batteries, *Carbon*, 2021, **179**, 33-41.

16 S. Liang, H. Shi, Z. Yu, Q. Liu, K. Cai, J. Wang and Z. Xu, Uncovering the design principle of conversion-based anode for potassium ion batteries via dimension engineering, *Energy Storage Materials*, 2021, **34**, 536-544.

17 S.-B. Huang, Y.-Y. Hsieh, K.-T. Chen and H.-Y. Tuan, Flexible nanostructured potassium-ion batteries, *Chem. Eng. J.*, 2021, **416**, 127697.

18 R. Huang, J. Lin, J. Zhou, E. Fan, X. Zhang, R. Chen, F. Wu and L. Li, Hierarchical Triple-Shelled $MnCo_2O_4$ Hollow Microspheres as High-Performance Anode Materials for Potassium-Ion Batteries, *Small*, 2021, **17**, 2007597.

19 D. Adekoya, H. Chen, H. Y. Hoh, T. Gould, M. J. T. Balogun, C. Lai, H. Zhao and S. Zhang, Hierarchical Co_3O_4@N-Doped Carbon Composite as an Advanced Anode Material for Ultrastable Potassium Storage, *ACS Nano*, 2020, **14**, 5027-5035.

20 Z. Sun, Y. Liu, W. Ye, J. Zhang, Y. Wang, Y. Lin, L. Hou, M. S. Wang and C. Yuan, Unveiling Intrinsic Potassium Storage Behaviors of Hierarchical Nano Bi@N-Doped Carbon Nanocages Framework via In Situ Characterizations, *Angew Chem Int Ed Engl*, 2021, **60**, 7180-7187.

21 N. Hussain, M. Li, B. Tian and H. Wang, Co_3Se_4 Quantum Dots as an Ultrastable Host Material for Potassium-Ion Intercalation, *Adv Mater*, 2021, **33**, 2102164.

22 J. Hu, Y. Xie, J. Zheng, Y. Lai and Z. Zhang, Unveiling nanoplates-assembled Bi_2MoO_6 microsphere as a novel anode material for high performance potassium-ion batteries, *Nano Research*, 2020, **13**, 2650-2657.

23 Q. Peng, S. Zhang, H. Yang, B. Sheng, R. Xu, Q. Wang and Y. Yu, Boosting Potassium Storage Performance of the Cu_2S Anode via Morphology Engineering and Electrolyte Chemistry, *ACS Nano*, 2020, **14**, 6024-6033

24 Q. Liu, F. Han, J. Zhou, Y. Li, L. Chen, F. Zhang, D. Zhou, C. Ye, J. Yang, X. Wu and J. Liu, Boosting the Potassium-Ion Storage Performance in Soft Carbon Anodes by the Synergistic Effect of Optimized Molten Salt Medium and N/S Dual-Doping, *ACS Appl Mater Interfaces*, 2020, **12**, 20838-20848.

25 Q. Yang, Z. Tai, Q. Xia, W. Lai, W. Wang, B. Zhang, Z. Yan, J. Peng, H. Yang, H. Liu, Q. Gu, S. Chou and H. Liu, Copper phosphide as a promising anode material for potassium-ion batteries, *J. Mater. Chem. A*, 2021, **9**, 8378-8385.

26 C. Huang, A. Xu, G. Li, H. Sun, S. Wu, Z. Xu and Y. Yan, Alloyed BiSb Nanoparticles Confined in Tremella-Like Carbon Microspheres for Ultralong-Life Potassium Ion Batteries, *Small*, 2021, **17**, 2100685.

27 J. Hu, Y. Xie, J. Zheng, H. Li, T. Wang, Y. Lai and Z. Zhang, Encapsulating V_2O_3 Nanoparticles in Hierarchical Porous Carbon Nanosheets via C-O-V Bonds for Fast and Durable Potassium-Ion Storage, *ACS Appl Mater Interfaces*, 2021, **13**, 12149-12158.

28 J. Lu, C. Wang, G. Xia, H. Tong, Y. Yang, D. Zhu and Q. Chen, A robust spring-like lamellar VO/C nanostructure for high-rate and long-life potassium-ion

batteries, *J. Mater. Chem. A*, 2020, **8**, 23939-23946.